

# Alzheimer's-related endosome dysfunction in Down syndrome is A $\beta$ -independent but requires APP and is reversed by BACE-1 inhibition

Ying Jiang<sup>a,b</sup>, Kerry A. Mullaney<sup>a</sup>, Corrinne M. Peterhoff<sup>a</sup>, Shaoli Che<sup>a,b</sup>, Stephen D. Schmidt<sup>a</sup>, Anne Boyer-Boiteau<sup>c</sup>, Stephen D. Ginsberg<sup>a,b,d</sup>, Anne M. Cataldo<sup>c,e</sup>, Paul M. Mathews<sup>a,b,f</sup>, and Ralph A. Nixon<sup>a,b,f,1</sup>

<sup>a</sup>Center for Dementia Research, Nathan Kline Institute, Orangeburg, NY 10962; Departments of <sup>b</sup>Psychiatry, <sup>d</sup>Physiology and Neuroscience, and <sup>f</sup>Cell Biology, Langone School of Medicine, New York University, New York, NY 10016, <sup>c</sup>Laboratory for Molecular Neuropathology, Mailman Research Center, McLean Hospital, Belmont, MA 02478; and <sup>e</sup>Department of Psychiatry and Neuropathology, Harvard Medical School, Boston, MA 02115

Edited by David D. Sabatini, New York University School of Medicine, New York, NY, and approved November 18, 2009 (received for review August 12, 2009)

**An additional copy of the  $\beta$ -amyloid precursor protein (APP) gene causes early-onset Alzheimer's disease (AD) in trisomy 21 (DS). Endosome dysfunction develops very early in DS and AD and has been implicated in the mechanism of neurodegeneration. Here, we show that morphological and functional endocytic abnormalities in fibroblasts from individuals with DS are reversed by lowering the expression of APP or  $\beta$ -APP-cleaving enzyme 1 (BACE-1) using short hairpin RNA constructs. By contrast, endosomal pathology can be induced in normal disomic (2N) fibroblasts by overexpressing APP or the C-terminal APP fragment generated by BACE-1 ( $\beta$ CTF), all of which elevate the levels of  $\beta$ CTFs. Expression of a mutant form of APP that cannot undergo  $\beta$ -cleavage had no effect on endosomes. Pharmacological inhibition of APP  $\gamma$ -secretase, which markedly reduced A $\beta$  production but raised  $\beta$ CTF levels, also induced AD-like endosome dysfunction in 2N fibroblasts and worsened this pathology in DS fibroblasts. These findings strongly implicate APP and the  $\beta$ CTF of APP, and exclude A $\beta$  and the  $\alpha$ CTF, as the cause of endocytic pathway dysfunction in DS and AD, underscoring the potential multifaceted value of BACE-1 inhibition in AD therapeutics.**

Alzheimer's disease | amyloid precursor protein | endocytosis | endosome

One of the pathological hallmarks of Alzheimer's disease (AD) is the presence of senile plaques containing fibrillar aggregates of the  $\beta$ -amyloid peptide (A $\beta$ ), a 40- to 43-amino acid peptide derived by cleavage of the  $\beta$ -amyloid precursor protein (APP) (1). Mutations of APP are known to cause early-onset familial AD (FAD) (2), and increased APP expression is considered a contributing factor in sporadic AD (SAD) (3). APP promoter polymorphisms associated with increased APP expression also cause early-onset AD (4). An additional copy of the *App* gene (duplication) is sufficient to cause early-onset autosomal dominant AD with cerebral amyloid angiopathy (CAA) (5, 6). These findings reinforce a longstanding hypothesis that the additional *App* gene found on the trisomic copy of human chromosome 21 (HSA21) in Down syndrome (DS) plays a critical role in the invariant early development of AD in DS individuals (7).

Early endosomes support the growth, homeostasis, and synaptic functions of neurons by sorting internalized cargoes to late endosomes and lysosomes for degradation, recycling selected constituents back to the plasma membrane, or delivering other cargoes to the Golgi for utilization (8). Early in AD, neuronal endosomes are abnormally enlarged (9), as they are in DS (10), enlargement that is likely to result in endosomal dysfunction (10) and subsequent neuronal vulnerability (8). APP, key APP proteolytic enzymes [i.e.,  $\beta$ -APP cleaving enzyme 1 (BACE-1) and  $\gamma$ -secretase], and various APP proteolytic fragments [i.e., A $\beta$  and a transmembrane, carboxyl-terminal APP fragment generated by BACE-1 ( $\beta$ CTF)] are all present in early endosomes (11, 12), raising the possibility that altered APP processing and early endosomal dysfunction are interrelated in AD.  $\beta$ -Cleavage of

APP, mediated by BACE-1, occurs within the luminal domain of APP in endocytic compartments and generates 2 APP fragments: a large, soluble amino-terminal fragment (sAPP $\beta$ ) that is secreted from the cells and  $\beta$ CTF containing the whole A $\beta$  peptide that remains associated with the cell (13). An alternative pathway involves the cleavage of APP 16 residues downstream of this site at the  $\alpha$ -cleavage site, which is mediated primarily by cell-surface metalloproteases (14). A $\beta$  is generated from the  $\beta$ CTF by an intramembrane cleavage mediated by the presenilin (PS)  $\gamma$ -secretase complex (13). Evidence supporting a pathological relationship between APP and endosomal function comes from the Ts65Dn mouse model of DS, which carries an extra copy of  $\sim$ 185 genes located on a region of mouse chromosome 16 (MMU16) orthologous to the "DS critical region" of HSA21 that is required for development of DS (15). These mice display key gross morphological features resembling human DS, and adult mice develop AD-related endosomal pathology, such as intraneuronal A $\beta$  accumulation and degeneration of basal forebrain cholinergic neurons (16). The extra copy of the *App* gene in this DS model is required for development of AD-related endocytic pathology and cholinergic neurodegeneration (17). Primary fibroblasts from individuals with DS display endosomal abnormalities similar to those seen in neurons of AD and DS patients (10), allowing us to investigate the relationship between elevated APP expression and endosomal pathology using APP overexpression, short hairpin RNA knockdown, and APP secretase inhibitors to modulate APP and APP metabolite levels in fibroblasts.

## Results

**APP Overexpression and Altered Endosomal Morphology in DS Fibroblasts.** Real-time qPCR analyses of fibroblasts from DS individuals of varying ages (17 weeks to 40 years) and age-matched 2N fibroblasts in DS fibroblasts showed the predicted  $\sim$ 1.5-fold increase in APP mRNA levels ( $P < 0.01$ ) as well as in mRNA levels for superoxide dismutase 1 (*SOD1*), a gene located on HSA21 ( $P < 0.01$ ). For actin, a gene not located on HSA21, mRNA levels were similar (Fig. 1A). Western blot analysis also revealed a similar increase in the levels of APP and SOD1 protein in DS fibroblasts (Fig. 1B). In our prior studies, we extensively used antibodies to early endosomal antigen-1 (EEA1) to identify and characterize

Author contributions: Y.J., S.D.G., P.M.M., and R.A.N. designed research; Y.J., K.A.M., C.M.P., S.C., S.D.S., A.B.-B., S.D.G., and A.M.C. performed research; A.M.C. contributed new reagents/analytic tools; Y.J., K.A.M., C.M.P., S.C., S.D.S., S.D.G., A.M.C., P.M.M. and R.A.N. analyzed data; and Y.J., P.M.M., and R.A.N. wrote the paper.

The authors declare no conflict of interest.

This article is a PNAS Direct Submission.

See Commentary on page 1263.

<sup>1</sup>To whom correspondence should be addressed at: Center for Dementia Research, Nathan Kline Institute, 140 Old Orangeburg Road, Orangeburg, NY 10962 or Departments of Psychiatry and Cell Biology, Langone Medical Center, New York University, 550 First Street, New York, NY 10016. E-mail: Nixon@NKI.RFMH.org.

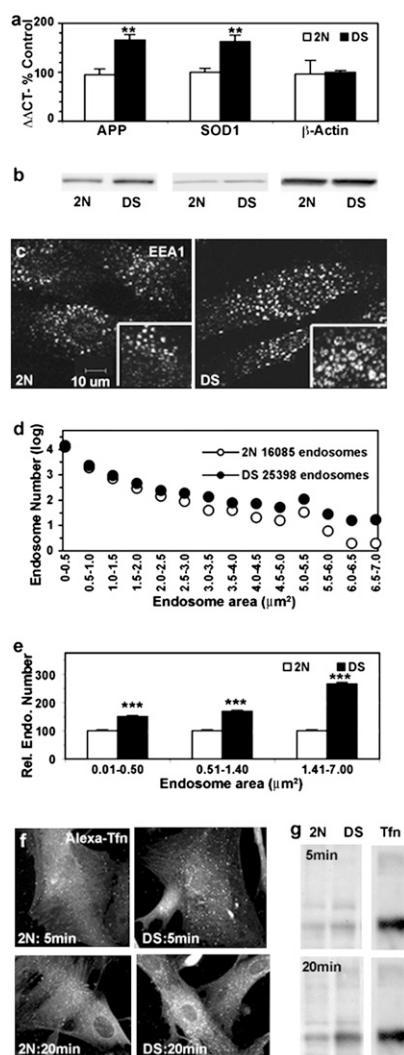


**Fig. 1.** Assessment of DS fibroblasts ( $n = 5$ ) compared with age-matched control samples ( $n = 5$ ). (A) Expression levels of APP, SOD1, and  $\alpha$ -actin in 2N and DS fibroblasts were determined by real-time qPCR (see *Materials and Methods*). \*\*,  $P < 0.01$ . (B) Representative Western blot analysis of APP and SOD1 expression in DS and 2N fibroblasts. (C) Immunofluorescence images showing EEA1-labeled early endosomes in representative 2N and DS fibroblasts, with high magnification image shown in *Inset*. (D and E) The sizes of EEA1-positive vesicles in DS and 2N fibroblasts were counted with Image J, calculated, and graphed. Shown are the total number of EEA1-positive endosomes from 4 DS and 4 2N fibroblast lines and their distributions according to size (D) and the relative numbers of endosomes of different size ranges (E; mean  $\pm$  SEM,  $n = 84$ ; \*\*\*,  $P < 0.001$ ). Immunolabeling (F) and Western blot analysis (G) showing transferrin uptake by 2N and DS fibroblast at 5 and 20 min.

early endosomes in brain tissue and cells in culture (9, 10). By immunofluorescence labeling, EEA1-positive endosomes were found to be substantially larger in DS fibroblasts (Fig. 1C), as previously reported (10). We compared the number and size of EEA1-positive endosomes from 4 2N and 4 DS fibroblast lines using morphometric analysis with Image J software in a total of 168 fibroblasts selected at random. EEA1-positive endosomes were 60% more numerous and 230% larger in DS fibroblasts than in 2N fibroblasts (Fig. 1D). Distribution analysis of endosome sizes revealed that the number of large ( $>1.41 \mu\text{m}^2$ ) endosomes was increased disproportionately (2.5-fold,  $P < 0.001$ ) in DS fibroblasts (Fig. 1E) relative to 2N fibroblasts, similar to the distribution pattern we previously reported in neurons in AD and DS brains (17).

In our earlier study of DS fibroblasts, we showed that endosomal enlargement reflected alterations in endocytic function (10). Using a similar transferrin assay to assess the rate of uptake of transferrin by reception-mediated endocytosis, we found qualitatively higher transferrin labeling in DS fibroblasts than in 2N fibroblasts beginning at 5 min to 20 min following uptake (Fig. 1F). These morphological observations were confirmed by Western blot analyses showing elevated transferrin uptake in DS fibroblasts (Fig. 1G).

**Reduction in APP and SOD1 Expression by siRNA and shRNA.** Using Qiagen's web siRNA-designing tool, we designed 21-bp siRNAs targeted to human *App* and, as a control, to *SOD1*. Immunofluorescence labeling with a C-terminal anti-APP antibody that detects full-length APP,  $\beta$ CTFs, and  $\alpha$ CTFs (C1/6.1, ref. 18) and anti-SOD1 antibody showed a qualitative decrease in the expression of APP or SOD1 in more than 80% of fibroblasts following transfection (Fig. 2A and C). Both siAPP and siSOD1 decreased the expression of the respective target protein by more than 50% in DS fibroblasts 48 h after transfection, whereas actin expression remained unchanged (Fig. 2B and D). Again, we measured the change in transferrin uptake in DS fibroblasts after the highly efficient *App* siRNA transfection. Western blot analyses following 5 min and 20 min of transferrin uptake showed a decreased level of endocytosis in DS fibroblasts treated with siAPP compared with fibroblasts treated with an irrelevant control siRNA ( $P < 0.05$ ) at the 20-min point (Fig. 2E and F).

Because RNA inhibition with shRNA has been shown to have advantages over siRNA, including less cytotoxicity associated with the silencing procedures (19) and the ability to use a GFP transfection marker to identify cells individually for subsequent morphological analyses, we generated hairpin RNA sequences to target *App* using the siAPP and siSOD1 sequences validated above. Immunofluorescence labeling revealed decreased APP expression in shAPP-transfected fibroblasts when double-labeled with anti-GFP and C1/6.1 (Fig. 2G). Similarly, SOD1 expression was down-regulated in shSOD1-transfected fibroblasts (Fig. 2I). As expected, transfection with vector only, which served as a negative control, produced no change in the expression of either APP or SOD1 in DS fibroblasts (Fig. 2H and J).

**Endosomal Defects in DS Fibroblasts Are Reversed by Lowering APP Levels.** To investigate the relationship between APP levels and the development of endosomal abnormalities, DS fibroblasts were transfected with shAPP and, after 48 h, were fixed and double-immunolabeled with anti-GFP and anti-EEA1 antibodies. As shown in Fig. 3A, shAPP transfection in DS fibroblasts restored both the number and size of EEA1-positive endosomes to the levels seen in 2N control fibroblasts (compare with Fig. 1). An analysis of the size distribution of endosomes revealed that shAPP transfection of DS fibroblasts reduced endosomal size and, in particular, the size of the largest early endosomes (70% decrease in endosomes  $> 1.41 \mu\text{m}^2$  in size,  $P < 0.001$ , versus 50% decrease in endosomes  $< 0.51 \mu\text{m}^2$  in size,  $P < 0.001$ ) (Fig. 3C). Neither shSOD1 nor a second control shRNA to calpastatin (Fig. 3B), a gene not located on HSA21, altered the numbers or sizes of EEA1-positive endosomes (Fig. 3D), showing the specificity of the shAPP for the endosomal pathology. Changes in the number and sizes of endosomes were less dramatic in 2N fibroblasts transfected in a similar manner with shAPP (Fig. 3E). In 2N fibroblasts, a uniform size reduction of 40% was seen in endosomes of all sizes (Fig. 3F).

**Overexpression of APP Induces AD-like Endosome Pathology in 2N Fibroblasts.** To establish further the influence of APP levels on the development of endosome pathology, we transfected 2N fibroblasts with dsRed-APP (wild-type APP) or with dsRed APPm596v, a mutated form of APP that lacks the amino acid sequence required for  $\beta$ -site cleavage (20). Cell lysates were collected for protein analysis, and cells were fixed for immunolabeling 48 h after

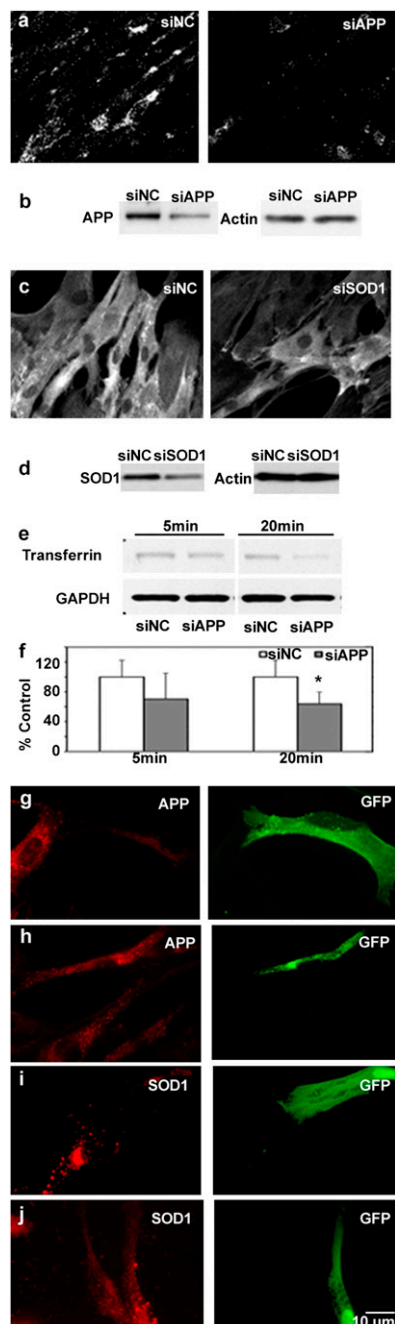


**Fig. 2.** Down-regulation of APP and SOD1 expression in DS fibroblasts by siRNA and shRNA leads to reversal of endocytic dysfunction. (A) C1/6.1 immunolabeling shows DS fibroblasts transfected with siNC and siAPP. (B) Western blot analysis shows expression of APP in siAPP-treated DS fibroblasts. (C) Immunolabeling and (D) Western blot analysis with anti-SOD1 shows expression of SOD1 in siSOD1-transfected DS fibroblasts. (E) Representative Western blot analysis of transferrin uptake at 5 and 20 min in siAPP-treated DS fibroblasts. (F) Mean level of transferrin uptake from 3 experiments. \*,  $P < 0.05$ . Expression of APP is shown in DS fibroblasts treated with shAPP (G) and vector (H). Expression of SOD1 is shown in shSOD1- (I) and vector- (J) transfected DS fibroblasts. In J the brightness levels of the red channel have been adjusted.

transfection. By Western blot analysis, 2N fibroblasts transfected with dsRed-APP or dsRed-APPm596v showed increased expression of full-length APP and APP-CTFs (Fig. 4A). The abundance of  $\beta$ CTF increased substantially in cells overexpressing dsRed-APP but was significantly lower and close to control levels in cells expressing the dsRed-APPm596v construct, confirming the

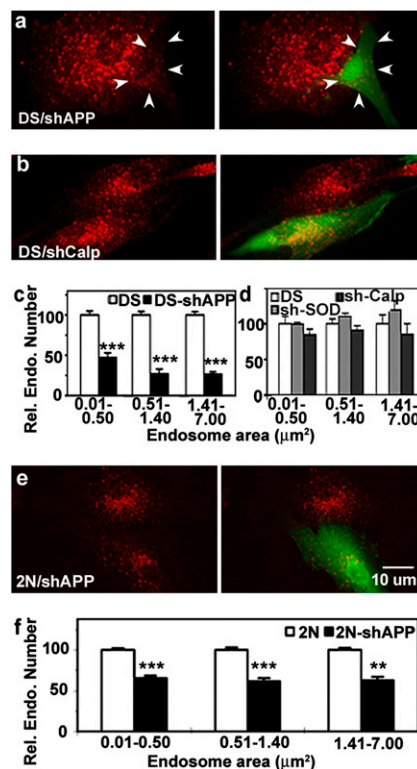


**Fig. 3.** Altered early endosomal morphology in DS fibroblasts transfected with shAPP. Anti-GFP antibody (green) identifies transfected fibroblasts (arrowhead), whereas anti-EEA1 antibody (red) identifies early endosomes. Shown is the immunolabeling of DS fibroblasts transfected with shAPP (A) and shCalpastatin (B) with EEA1 (Left) and EEA1 plus GFP (Right). EEA1-positive endosomes in DS fibroblasts transfected with either shAPP (C) or shSOD1/shCalpastatin (D) were counted and analyzed with Image J. The bar graphs present the mean  $\pm$  SEM for relative numbers of endosomes in different size ranges.  $n = 80, 55,$  and  $50$  for shAPP-, shSOD1-, and shCalpastatin-transfected DS fibroblasts, respectively. \*\*\*,  $P < 0.001$ . 2N fibroblasts also were treated with shAPP (E), and endosomal size was determined as above (F).  $n = 63$ ; \*\*,  $P < 0.01$ ; \*\*\*,  $P < 0.001$ .

reduction of  $\beta$ -cleavage of APP. Notably, the  $\beta$ -cleavage mutation did not appreciably affect  $\alpha$ CTF levels. EEA1-positive endosomes were significantly enlarged in dsRed-APP-transfected 2N fibroblasts (Fig. 4B) but remained unaltered in size in cells transfected with dsRed-APPm596v (Fig. 4C). Morphometric analysis of endosomal number and size showed that the numbers and sizes of endosomes in dsRed-APP transfected 2N fibroblasts were comparable to those seen in DS fibroblasts (compare with Fig. 1E). Furthermore, the number of the largest size endosomes ( $> 0.51 \mu\text{m}^2$ ) was increased 3.5-fold ( $P < 0.001$ ) over that in 2N fibroblasts (Fig. 4D), an abnormal increase comparable to that seen in DS fibroblasts (Fig. 1E). The observation that the overexpression-mutated form of APP had no effect on the size of endosomes established the importance of APP  $\beta$ -cleavage and its product  $\beta$ CTF in causing AD-related endosome abnormalities. This result also eliminated  $\alpha$ CTF as the cause, because transfection of cells with mutated APP had a minimal effect on levels of  $\alpha$ CTF (Fig. 4A) (20).

**APP  $\gamma$ -Secretase Inhibition Does Not Rescue AD-like Endosomal Pathology in DS Fibroblasts and Induces This Pathology in 2N Fibroblasts.** Evidence from human AD brain and the Ts65Dn mouse model of DS suggested that A $\beta$  is not causally related to AD-related endosomal enlargement (17, 21). To address this issue further, we used a  $\gamma$ -secretase inhibitor to inhibit A $\beta$  pro-

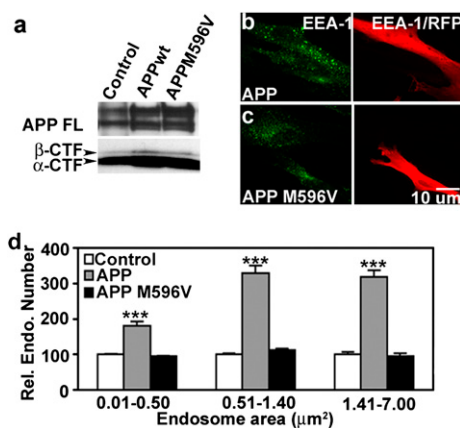


**Fig. 4.** APP overexpression in 2N fibroblasts induces AD-like endosome pathology. (A) Western blot of 2N fibroblast lysates collected 48 h after transfection with either dsRed-APP or dsRed-APPm596v was probed with antibody C1/6.1. Double-labeling for RFP and EEA1 shows EEA1-positive endosomes in APP- (B) and APPm596v- (C) transfected (RFP-positive) and nontransfected (RFP-negative) 2N fibroblasts. (D) Relative number of EEA1-positive endosomes of different size ranges in 2N fibroblasts overexpressing APP or APPm596v (mean  $\pm$  SEM,  $n = 100$ ). \*\*\*,  $P < 0.001$ .

duction in the human fibroblasts. Using an A $\beta$  ELISA, we demonstrated, as previously observed with this inhibitor (L685,458, 10  $\mu\text{M}$ ; Peptide International) (22), that levels of A $\beta$ 40 and A $\beta$ 42 in the culture media were significantly lowered after 18 h of exposure (Fig. 5A) (A $\beta$ 40,  $P < 0.01$ ; A $\beta$ 42,  $P < 0.05$ ). Western blot analysis showed that the levels of APP remained unchanged but that CTFs, including  $\beta$ CTF, increased markedly in these fibroblasts (Fig. 5B). Despite lowered levels of A $\beta$ , the size and number of EEA1-positive endosomes were increased (Fig. 5C and D), resembling those seen in untreated DS fibroblasts (Fig. 1C). Fig. 5E shows that endosome number increased disproportionately (3.5-fold,  $P < 0.001$ ) in the larger-size groups ( $>1.41 \mu\text{m}^2$ ). In contrast to 2N fibroblasts, the  $\gamma$ -secretase inhibitor had no statistically significant effect on EEA1-positive endosomes in DS fibroblasts (1.3-fold,  $P = 0.44$ , for endosomes  $>1.41 \mu\text{m}^2$ ). Furthermore, the increase seen on 2N fibroblasts treated with  $\gamma$ -secretase inhibitor was diminished in 2N fibroblasts positively transfected with shAPP (Fig. 5F), indicating that the effects of  $\gamma$ -secretase inhibitor on endosomes are APP-dependent. In 2N fibroblasts pretreated with the inhibitor for 18 h, transferrin uptake was increased significantly as compared with control 2N fibroblasts ( $P < 0.01$ ) (Fig. 5G and H).

**Elevating  $\beta$ CTF Induces AD-like Endosomal Pathology in 2N Fibroblasts.** To confirm the effect of increased  $\beta$ CTF levels in driving endosome enlargement, 2N fibroblasts were transfected with a construct consisting of the  $\beta$ CTF linked at its C terminus to GFP, a construct that has been shown to localize appropriately within the cell and undergo subsequent  $\gamma$ -secretase cleavage to yield an APP intracellular domain (AICD) linked to GFP (23). Expression and  $\gamma$ -secretase processing of this construct were verified by Western blot analysis (Fig. 6A). Increased  $\beta$ CTF immunolabeling, including puncta consistent with vesicular compartments, was seen in transfected fibroblasts, with the AICD GFP  $\gamma$ -secretase product accumulating in the cytosol (Fig. 6B) (23). Transfected 2N fibroblasts exhibited an increase in endosomal size (Fig. 6C), with larger endosomes ( $>1.41 \mu\text{m}^2$ ) showing the greatest increase (3-fold,  $P < 0.001$ ) (Fig. 6D), suggesting that elevation of  $\beta$ CTF levels alone can produce effects on endosomal size similar to those of increased APP expression.

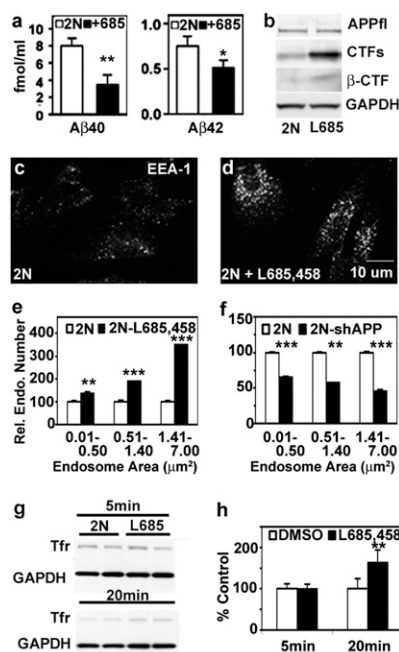


**Fig. 5.**  $\gamma$ -Secretase inhibition using L685,458 induces the AD-like endosomal phenotype in 2N fibroblasts. (A) A $\beta$ -40 and A $\beta$ -42 levels in cell-culture media collected 18 h after incubation with 10  $\mu\text{M}$  of L685,458 were determined by ELISA (\*,  $P < 0.05$ ; \*\* $P < 0.01$ ). (B) Western blot analysis of cell lysates probed by C1/6.1 for APP and CTFs and by 6E10 for  $\beta$ CTF. Immunolabeling showed EEA1-positive vesicles in (C) DMSO- and (D) L685,458-treated fibroblasts. (E) The relative number of endosomes of different size ranges (mean  $\pm$  SEM,  $n = 90$ ; \*\*,  $P < 0.01$ ; \*\*\*,  $P < 0.001$ ) in DMSO- and L685,458-treated 2N fibroblasts. (F) The relative number of endosomes of different size ranges (mean  $\pm$  SEM,  $n = 74$ ; \*\*,  $P < 0.01$ ; \*\*\*,  $P < 0.001$ ) in shAPP-transfected and untransfected 2N fibroblasts. Western blot analysis (G) and its quantitation (H) of transferrin uptake in L685,458-treated versus control 2N fibroblasts normalized to GAPDH at 5 and 20 min. \*\*,  $P < 0.01$ .

**Reduced BACE-1 Expression Rescues Endosome Pathology in DS Fibroblasts.** To demonstrate further that the  $\beta$ CTF is required for the development of AD-related endosome dysfunction, DS fibroblasts were treated with a previously characterized shRNA construct (pSilencer:BACE-1.1) (24) to lower the expression of BACE-1 and thus the production of  $\beta$ CTFs. Compared with DS fibroblasts treated with vector only (Fig. 7A), fibroblasts transfected with shBACE1 showed a 30% reduction in A $\beta$  secretion and a significant decrease in the size of EEA1-positive endosomes (Fig. 7B). Similar to the DS fibroblasts transfected with shAPP, the reduction in endosome size occurred disproportionately in the largest endosomes ( $>1.41 \mu\text{m}^2$ ) ( $P < 0.001$ ) (Fig. 7C).

## Discussion

We have shown here that elevated APP expression in fibroblasts from DS individuals is necessary and sufficient to cause morphological and functional abnormalities of early endosomes closely resembling those seen as the earliest neuronal pathology in AD patients (10). These results are significant in light of observations that an extra copy of *App* promotes early-onset AD in DS individuals (7) and that duplication of the *App* locus alone has been found to cause FAD (5, 6). Moreover, even mild (20%) APP overexpression increases AD risk in the general population (7), and, interestingly, trisomy 21 mosaicism often is associated with AD (25). Although increased A $\beta$  production in the brain is likely to be a consequence of increased *App* gene copy, our findings also strongly link overexpression of APP and generation of  $\beta$ CTF to pathological endosomal effects that are not mediated by A $\beta$  but likely contribute to neuronal vulnerability and disease (26).

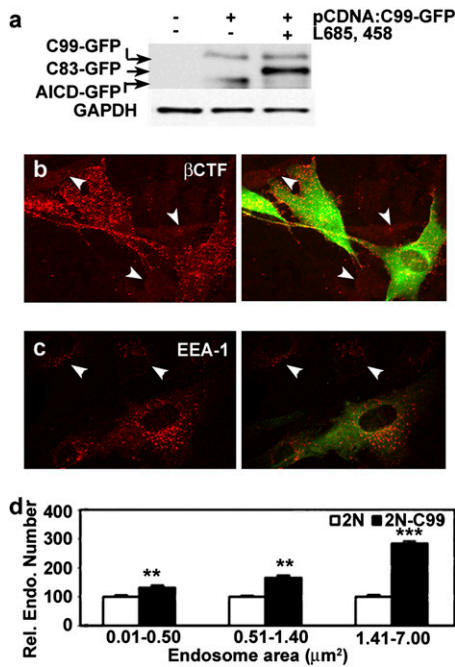


**Fig. 6.** Overexpression of a  $\beta$ CTF construct induces the AD-like endosomal phenotype in 2N fibroblasts. (A) Western blot of C1/6.1 of 2N fibroblasts transfected with pcDNA3:C99-GFP. Immunolabeling with anti-EEA1, N25, and anti-GFP antibodies shows  $\beta$ CTF (B) and EEA1 (C) in transfected and nontransfected (arrowhead) 2N fibroblasts. (D) Relative numbers of endosomes in transfected and nontransfected 2N fibroblasts (mean  $\pm$  SEM,  $n = 55$ ). \*\*,  $P < 0.01$ ; \*\*\*,  $P < 0.001$ .

In our study, shRNA against APP effectively reduced APP expression in DS fibroblasts and reversed the AD-related early endosome phenotype in DS fibroblasts. By contrast, endosomal pathology was not reversed when several other genes were silenced, including *SOD1*, a gene located in the trisomic region of HSA21, and

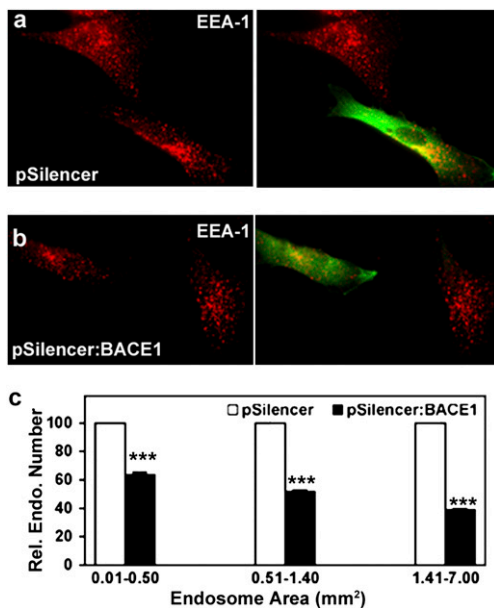


**Fig. 7.** Altered early endosomal morphology in DS fibroblasts transfected with pSilencer: BACE-1. Immunolabeling showed EEA1-positive vesicle in pSilencer- (A) and shBACE1- (B) transfected DS fibroblasts, with cotransfection of pGFP as a marker for transfection. The contrast levels have been adjusted in B. (C) Sizes of EEA1-positive vesicles in vector and shBACE1-transfected fibroblasts were calculated and graphed (mean  $\pm$  SEM,  $n = 52$ ). \*\*\*,  $P < 0.001$ .

calpastatin, which is not located on HSA21. Our observations in DS fibroblasts agree with findings in Ts65Dn mice, in which selective deletion of 1 copy of *App* or a small portion of the MNU16 segment containing *App* reverses both neuronal endosomal pathology (17) and degenerative changes in basal forebrain cholinergic neuron (16).

Despite its dependence on elevated APP levels, endosome dysfunction in DS fibroblasts was not blocked by lowering  $A\beta$  production with a  $\gamma$ -secretase inhibitor, supporting previous evidence in AD and mouse AD models that endosome pathology is not  $A\beta$ -dependent (16). In FAD brain from individuals with presenilin mutations, for example, neuronal endosomes are not abnormally enlarged despite abundant  $\beta$ -amyloid deposition, consistent with other evidence that pathogenic mechanisms in PS-FAD may involve APP trafficking pathways other than the endocytic pathway (27). Moreover, in Ts65Dn mice, endosomes are pathologically enlarged even though  $A\beta$  is not elevated (16, 17, 21). Indeed, multiple lines of evidence from our study implicate the  $\beta$ CTF of APP in the development of endosome dysfunction in DS fibroblasts. Treatments of 2N fibroblasts that increased levels of either APP or  $\beta$ CTFs induced a pattern of endosomal changes similar to that seen in DS fibroblasts, whereas treatments that decreased APP or, more specifically,  $\beta$ CTFs reversed the endosomal dysfunction in DS fibroblasts. Thus, in all conditions studied,  $\beta$ CTF elevation is the single common APP-related alteration associated with abnormal endosome enlargement and proliferation and accelerated endocytosis.

The  $\beta$ CTF has been found to accumulate in early endosomes in cell models of AD pathology and in enlarged early endosomes of AD brain (28).  $\beta$ CTF increases membrane conductances in a concentration-dependent fashion and is more effective than  $A\beta$  in forming channels in the plasma membrane (29), suggesting that  $\beta$ CTF can disrupt neuronal ionic homeostasis. Additionally, lowering BACE-1 levels with siRNA reduces the neurodegenerative and behavioral deficits in APP transgenic mice (30). Both  $\beta$ CTF and BACE-1 are abundant in early endosomes (31), and both are elevated in the brains of DS individuals (32).

Neurons are particularly dependent on endocytosis for maintaining the structure of dendrites and axons and supporting synaptic transmission and regulation of receptors molecules critical for neuronal survival and repair as well as efficient uptake and intracellular delivery of lipids (26). Our results link a genetic defect responsible for early-onset forms of AD directly to endocytic pathway dysfunction, which is the earliest described neuronal pathology in AD. We have shown that AD-related endosome dysfunction in DS is dependent on APP levels and elevated levels of the  $\beta$ CTF but is independent of  $A\beta$  or  $\alpha$ CTF levels. Thus, our findings implicate the BACE-1-cleaved  $\beta$ CTF of APP, but not  $A\beta$ , in the development of endosomal pathology in early-onset AD. In conclusion, our findings suggest that multiple APP metabolites, undoubtedly including but not limited to  $A\beta$ , are likely to contribute to the pathobiology of AD.

## Materials and Methods.

**siRNA Synthesis and shRNA Plasmid Construction.** In vitro synthesis of siRNA was performed using a commercially available kit (Silencer siRNA Construction Kit; Applied Biosystems). DNA templates of targeted APP and *SOD1* RNA sites were ordered from Qiagen for the synthesis of siRNA according to the Ambion protocol. Multiple sequences for siRNA constructs were made for *App* and *Sod1*. The most effective siRNA sequence was AACATGCACATGAATGCCAG for *App* and AATGTGACTGCTGACAAAGAT for *SOD1*. These siRNA sequences also were used as inserts for construction of GFP-tagged shRNAs expressed in an shRNA-GFP (kindly provided by Y. Wen, University of North Texas). The vector contains GFP as a marker, an H1RNA promoter, and a zeocin resistance gene for selection. pSilencer:BACE 1.1, a kind gift from L. H. Tsai (Massachusetts Institute of Technology) (24), was used to down-regulate the expression of *Bace1* in DS fibroblasts. pcDNA3:C99-GFP (the vector expressing the  $\beta$ CTF-GFP fusion protein) was kindly provided by C. Haass (Ludwig-Maximilian University) (23). A mutated form of APP construct (DsRed-APPm695v) was obtained by site-mutagenesis on dsRed-APP (a generous gift from S. Kim, Nathan Kline Institute) using Quik-

Change Lightning Site-Directed Mutagenesis Kit (Stratagene). siRNA negative control (siNC) was purchased from Applied Biosystems.

**Cell Culture and Transfections.** Human forearm skin fibroblasts from DS and diploid age-matched controls were purchased from the Coriell Cell Repositories and cultured according to the distributor's protocols (<http://ccr.coriell.org/>). Cell passage number ranged from p4 to p13, and cells at 85–90% confluency were used throughout the study. Fibroblasts were seeded on glass coverslips in 12-well dishes for immunolabeling or 6-well dishes for biochemical applications and cultured with antibiotic-free media 24 h before transfection. siPortAmine was used as the transfection agent for siRNA and siPortXP-1 was used for shRNA (Ambion). TransIT-LT1 agent (Mirus) was used for all other DNA plasmid transfections. Fibroblasts were fixed for immunolabeling or harvested for Western blot and qPCR analyses 48–72 h after transfection. A highly sensitive ELISA was used to determine levels of A $\beta$ -40 and A $\beta$ -42 in the cell-culture media (18).

**Quantitative PCR Analysis.** Approximately 1 million fibroblasts were seeded onto 100-mm culture dishes. Total RNA from fibroblasts was extracted 48 h later using TRIzol Reagent (Invitrogen). RNA quality and quantity were evaluated using the RNA 6000 Pico kit (Agilent Technologies). From each sample, 2  $\mu$ g of RNA was reverse-transcribed to cDNA with Taqman Reverse Transcription Reagents (Applied Biosystems), according to the manufacturer's protocol. Samples were loaded onto a 96-well optical PCR plate and assayed on a real-time PCR cycler (7900HT; Applied Biosystems) as described previously (33). The cycle threshold ( $C_T$ ) for each sample was detected and used to compare the gene expression level between samples using the difference between the cycle number ( $\Delta\Delta CT$ ) method with GAPDH as an endogenous control (33).

**Immunofluorescence Labeling.** For immunolabeling,  $5 \times 10^4$  fibroblasts per coverslip per well were seeded into a 12-well plate and grown to 80–90% confluence before transfection or other treatment. Cells were washed with PBS and fixed with 4% paraformaldehyde at room temperature for 20 min and probed with C1/6.1 (against the C terminus of APP) (18), N25 (against  $\beta$ CTF and A $\beta$ ) (34), or SOD1 (Santa Cruz Biotechnology Inc). Transfected fibroblasts were identified with anti-GFP antibody (Invitrogen) or anti-RFP (Abcam), whereas anti-EEA1 (BD Biosciences) was used to examine phenotypic changes in early endosomes (10). Alexa-Fluor 568 and Alexa-Fluoro

488 conjugated secondary antibody were from Invitrogen, and immunofluorescence images were obtained on a Zeiss Axiovert 200 epifluorescent microscope.

**Western Blot Analysis.** Lysate was collected from fibroblasts, and equal amounts of protein were sized by SDS/PAGE as described previously (18). Various antibodies, including C1/6.1, 6E10 (Covance), anti-SOD1, anti- $\beta$ -actin (Sigma), anti-GAPDH (Santa Cruz), and anti-transferrin (AbCam) were used to detect levels of these specific proteins.

**Receptor-Mediated Uptake.** Receptor-mediated transferrin uptake in fibroblasts was performed as previously described (10). After various treatments, fibroblasts were washed with PBS followed by incubation with 0.1% BSA/PBS containing 20 mM Hepes (pH 7.4) at 37 °C for 30 min. The fibroblasts were incubated with 50  $\mu$ g/mL Alexa-568–tagged transferrin (Invitrogen) on ice for 1 h and then were washed and incubated at 37 °C for 5 or 20 min before being harvested for Western blot analysis.

**Quantitative Analysis of EEA1-Positive Endosomes.** The average size of EEA1-positive profiles in cultured fibroblasts after various treatments was determined by Image J, a Java image-processing program derived from the National Institutes of Health Image (<http://rsb.info.nih.gov/ij/>, 1997–2007). Immunofluorescence images of the fibroblasts were captured using a Zeiss microscope at 100 $\times$ , compiled and converted to 8-bit gray-scale within Image J. All images were scaled to the same threshold to ensure quantitative consistency. Randomly selected fibroblasts were analyzed with respect to total endosomal count (endosomal area in squared pixels). The endosomal area in squared pixels then was converted to the actual size in the measurement of square micrometers according to Zeiss AxioVision 4.6 (conversion factor = 0.09788  $\mu$ m/pixel). For each condition, endosomes from more than 20 fibroblasts were counted, totaled, and grouped based on their size (square micrometers) for statistical comparison by 2-tailed Student's *t*-tests.

**ACKNOWLEDGMENTS.** We are grateful to Nicole Piorkowski for assistance with manuscript preparation and to Seonil Kim for the dsRed-1 construct. This work was supported by National Institute on Aging Grant AG017617 (to R.A.N.).

- Haass C, et al. (1992) Amyloid beta-peptide is produced by cultured cells during normal metabolism. *Nature* 359:322–325.
- Golde TE, Estus S, Younkin LH, Selkoe DJ, Younkin SG (1992) Processing of the amyloid protein precursor to potentially amyloidogenic derivatives. *Science* 255:728–730.
- Sisodia SS, Price DL (1995) Role of the beta-amyloid protein in Alzheimer's disease. *FASEB J* 9:366–370.
- Athan ES, Lee JH, Arriaga A, Mayeux RP, Tycko B (2002) Polymorphisms in the promoter of the human APP gene: Functional evaluation and allele frequencies in Alzheimer disease. *Arch Neurol* 59:1793–1799.
- Rovelet-Lecrux A, et al. (2006) APP locus duplication causes autosomal dominant early-onset Alzheimer disease with cerebral amyloid angiopathy. *Nat Genet* 38:24–26.
- Sleegers K, et al. (2006) APP duplication is sufficient to cause early onset Alzheimer's dementia with cerebral amyloid angiopathy. *Brain* 129:2977–2983.
- Margallo-Lana M, et al. (2004) Influence of the amyloid precursor protein locus on dementia in Down syndrome. *Neurology* 62:1996–1998.
- Nixon RA (2004) Niemann-Pick Type C disease and Alzheimer's disease: The APP-endosome connection fattens up. *Am J Pathol* 164:757–761.
- Cataldo AM, et al. (2000) Endocytic pathway abnormalities precede amyloid beta deposition in sporadic Alzheimer's disease and Down syndrome: Differential effects of APOE genotype and presenilin mutations. *Am J Pathol* 157:277–286.
- Cataldo AM, et al. (2008) Down syndrome fibroblast model of Alzheimer-related endosome pathology: Accelerated endocytosis promotes late endocytic defects. *Am J Pathol* 173:370–384.
- Arbel M, Yacoby I, Solomon B (2005) Inhibition of amyloid precursor protein processing by  $\beta$ -secretase through site-directed antibodies. *Proc Natl Acad Sci USA* 102:7718–7723.
- Rajendran L, et al. (2008) Efficient inhibition of the Alzheimer's disease  $\beta$ -secretase by membrane targeting. *Science* 320:520–523.
- Hardy J, Selkoe DJ (2002) The amyloid hypothesis of Alzheimer's disease: Progress and problems on the road to therapeutics. *Science* 297:353–356.
- Sisodia SS (1992) Beta-amyloid precursor protein cleavage by a membrane-bound protease. *Proc Natl Acad Sci USA* 89:6075–6079.
- Holtzman DM, et al. (1996) Developmental abnormalities and age-related neurodegeneration in a mouse model of Down syndrome. *Proc Natl Acad Sci USA* 93:13333–13338.
- Salehi A, et al. (2006) Increased App expression in a mouse model of Down's syndrome disrupts NGF transport and causes cholinergic neuron degeneration. *Neuron* 51:29–42.
- Cataldo AM, et al. (2003) App gene dosage modulates endosomal abnormalities of Alzheimer's disease in a segmental trisomy 16 mouse model of Down syndrome. *J Neurosci* 23:6788–6792.
- Mathews PM, et al. (2002) Alzheimer's disease-related overexpression of the cation-dependent mannose 6-phosphate receptor increases A $\beta$  secretion: Role for altered lysosomal hydrolase distribution in beta-amyloidogenesis. *J Biol Chem* 277:5299–5307.
- Brummelkamp TR, Bernards R, Agami R (2002) A system for stable expression of short interfering RNAs in mammalian cells. *Science* 296:550–553.
- Citron M, Teplow DB, Selkoe DJ (1995) Generation of amyloid beta protein from its precursor is sequence specific. *Neuron* 14:661–670.
- Choi JH, et al. (2009) Age-dependent dysregulation of brain amyloid precursor protein in the Ts65Dn Down syndrome mouse model. *J Neurochem* 110:1818–1827.
- Wolfe MS, Esler WP, Das C (2002) Continuing strategies for inhibiting Alzheimer's gamma-secretase. *J Mol Neurosci* 19:83–87.
- Kaether C, Schmitt S, Willem M, Haass C (2006) Amyloid precursor protein and Notch intracellular domains are generated after transport of their precursors to the cell surface. *Traffic* 7:408–415.
- Kao SC, Krichevsky AM, Kosik KS, Tsai LH (2004) BACE1 suppression by RNA interference in primary cortical neurons. *J Biol Chem* 279:1942–1949.
- Geller LN, Potter H (1999) Chromosome missegregation and trisomy 21 mosaicism in Alzheimer's disease. *Neurobiol Dis* 6:167–179.
- Nixon RA (2005) Endosome function and dysfunction in Alzheimer's disease and other neurodegenerative diseases. *Neurobiol Aging* 26:373–382.
- Nixon RA (2007) Autophagy, amyloidogenesis and Alzheimer disease. *J Cell Sci* 120:4081–4091.
- Jin LW, Shie FS, Maezawa I, Vincent I, Bird T (2004) Intracellular accumulation of amyloidogenic fragments of amyloid-beta precursor protein in neurons with Niemann-Pick type C defects is associated with endosomal abnormalities. *Am J Pathol* 164:975–985.
- Kim HS, et al. (2000) Carboxyl-terminal fragment of Alzheimer's APP destabilizes calcium homeostasis and renders neuronal cells vulnerable to excitotoxicity. *FASEB J* 14:1508–1517.
- Singer O, et al. (2005) Targeting BACE1 with siRNAs ameliorates Alzheimer disease neuropathology in a transgenic model. *Nat Neurosci* 8:1343–1349.
- Vassar R, et al. (1999) Beta-secretase cleavage of Alzheimer's amyloid precursor protein by the transmembrane aspartic protease BACE. *Science* 286:735–741.
- Nistor M, et al. (2007) Alpha- and beta-secretase activity as a function of age and beta-amyloid in Down syndrome and normal brain. *Neurobiol Aging* 28:1493–1506.
- Ginsberg SD, Che S, Wu J, Counts SE, Mufson EJ (2006) Down regulation of trk but not p75NTR gene expression in single cholinergic basal forebrain neurons mark the progression of Alzheimer's disease. *J Neurochem* 97:475–487.
- Mathews PM, et al. (2002) Calpain activity regulates the cell surface distribution of amyloid precursor protein: Inhibition of calpains enhances endosomal generation of beta-cleaved C-terminal APP fragments. *J Biol Chem* 277:36415–36424.